

# A Spectral Geometrical Model for Compton Scatter Tomography Based on the SSS Approximation

**Kazantsev, Ivan G.; Olsen, Ulrik Lund; Poulsen, Henning Friis; Hansen, Per Christian**

*Published in:*
Proceedings of the The 4th International Conference on Image Formation in X-Ray Computed Tomography

*Publication date:*
2016

*Document Version*
Publisher's PDF, also known as Version of record

# A Spectral Geometrical Model for Compton Scatter Tomography Based on the SSS Approximation

Ivan G. Kazantsev
Institute of Computational Mathematics
and Mathematical Geophysics
Novosibirsk, Russia
Email: kazantsev.ivan6@gmail.com

Ulrik L. Olsen, Henning F. Poulsen
Department of Physics
Technical University of Denmark
Lyngby, Denmark
Emails: ullu@dtu.dk, hfpo@fysik.dtu.dk

Per C. Hansen
COMPUTE Department
Technical University of Denmark
Lyngby, Denmark
Email: pcha@dtu.dk

***Abstract*—The forward model of single scatter in the Positron Emission Tomography for a detector system possessing an excellent spectral resolution under idealized geometrical assumptions is investigated. This model has the form of integral equations describing a flux of photons emanating from the same annihilation event and undergoing a single scattering at a certain angle. The equations for single scatter calculation are derived using the Single Scatter Simulation approximation. We show that the three-dimensional slice-by-slice filtered backprojection algorithm is applicable for scatter data inversion provided some assumptions on the attenuation map are justified.**

## I. Introduction

The Compton scatter phenomenon is inherent of such tomographic imaging modalities as the X-ray transmission Computed Tomography (CT) [1], the Single Photon Emission Tomography (SPECT) [2] and the Positron Emission Tomography (PET) [3]. Many authors succesfully apply transmission CT algoritms for the Compton scatter imaging systems both with the external and the internal sources of radiation. It has been shown that SPECT can be considered as Compounded Conical Radon Transform [4], and PET as a perturbation of the X-ray transform [5]. In this paper we focus on the analytical aspects of deriving an idealized forward model of the Compton single scatter in the PET.

Idealized models of image formation in tomography are useful instruments for exploring the potentials and limits of reconstructive ability of data acquired in an imaging modality of interest. Usually having the form of an integral transform or differential equation, the idealized model is expected to answer the principal questions: whether the available noiseless data are sufficient to restore an object under investigation, to what extent the objects frequencies are recoverable, etc. In the case when an explicit inversion formula is not available, a discrete version of the idealized forward operator can be combined with algebraic iterative methods to answer these questions.

As compared to idealized models, there is comprehensive Monte Carlo (MC) statistical simulation in much more wide use. The MC modeling is able to take into account every technical detail of photon transport and detection phenomena and therefore there is a demand for computer resources. The MC statistical simulation (as well as physical phantom studies) are the 'gold standard' for verification of scatter modelling. Reference [3] states: "Nevertheless, the complexity and computing requirements of Monte Carlo simulation led to the development of analytical simulation tools based on simplifying approximations to improve speed of operation". Those analytical simulation tools are known as Single Scatter Simulation (SSS) and they have been proven to be fast and efficient in modeling the main scatter features together with discreteness of detectors and many other factors [6]. While the SSS model estimates a scatter flux detected within finite detector elements for a range of energies, the idealized model provides a sample value of a scatter for a given energy and detected at a given point of detector. That is, in the idealized model the detector system has an excellent energy resolution and the size of each detector element approaches zero. It is assumed that detectors count all incoming single scattered photons of a certain energy, or equivalently, the photons scattered once under a certain angle.

## II. Methods

The integral model of PET using primary photons [5] operates with internal sources of isotope activity $f(x,y,z)$ within a functionalizing medical object described by the known linear attenuation map $\mu(x,y,z)$ and a pair of detectors $A$ and $B$:

$$P^{AB} = \exp\left[-\int_A^B \mu(x',y',z')dl'\right]\int_A^B f(x,y,z)dl, \qquad (1)$$

where $dl$, $dl'$ are the elements of integration along $AB$. Equation (1) factorizes integrals over the activity $f$ and the attenuation $\mu$, thus reducing the problem to a classical X-ray CT provided that the data $P^{AB}$ undergoes attenuation correction. Then the data can be treated as integrals of $f$ along the lines of response, which are thought to be trajectories of propagation of primary (unscattered) photons with energy $E = 511$ keV. The support of the attenuation map $\mu$ is a domain $D(\mu)$, and the support of the activity function $f$ is a domain $D(f) \subset D(\mu)$ of unknown structure. The PET problem consists in reconstruction of the activity $f$ and its support $D(f)$ exploiting data $P^{AB}$, recorded by a multitude of detectors $(A,B)$ positioned around the object. A physical feature of PET is basically a huge amount of photon pairs $(u,v)$, collinearly traveling in opposite directions from the annihilation point $C$, where positron resulting from isotope

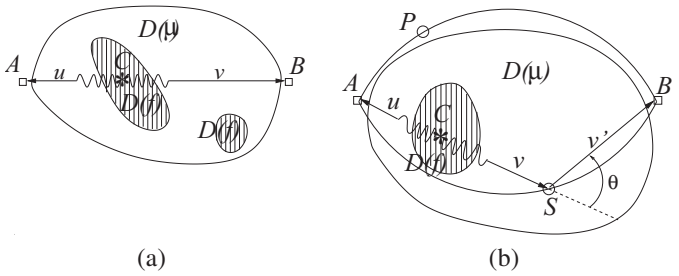


Fig. 1. (a) Primary photons $(u, v)$ of energy $E = 511$ keV, originating from annihilation point $C \in D(f)$. (b) Single Compton scatter happens in point $S \in D(\mu)$, $v'$ is a photon $v$ with energy $E'$, scattering with angle $\theta$. The $P$ is geometrically potential point for scatter with angle $\theta$, however it is out of domain $\mu$ ($P \notin D(\mu)$, $\mu(P) = 0$), therefore does not contribute to the $B$.

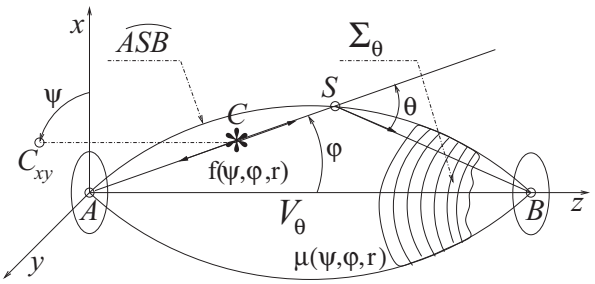


Fig. 2. A 3D geometric model of single scattering. Circular detectors are centered at the points $A$ and $B$; $S$ is a scattering point with the polar coordinates $(\psi, \varphi, |AS|)$ and the scatter angle $\theta$; $C_{xy}$ is a projection of $C$ onto the plane $xAy$; $C$ is an annihilation event. The surface $\Sigma_\theta$ is a loci of points $S$ of scatter under the angle $\theta$ and the spherical coordinates $(\psi, \varphi, |AS|)$, $\angle ABS = \theta - \varphi$.

decay meets some of free electons of the media $\mu$ (Figure 1 (a)). In addition to primary photons, there are the ones $v'$ with energies $E' < E$ that undergo the Compton scatter (Figure 1 (b)), and the energies are connected to the scattering angle $\theta$ by the Compton relation: $E' = E/(2 - \cos\theta)$.

### A. Single Scatter Simulation Approximation

The Single Scatter Simulation (SSS) technique [6] estimates the expected single scatter coincidence rate in the detector pair $(A, B)$ as an integral over the total scatter volume $V = D(\mu)$:

$$S_V^{AB} = \iiint_V dV \frac{\sigma_{AS}\sigma_{BS}}{4\pi|AS|^2|BS|^2} \frac{\mu}{\sigma_C} \frac{\partial\sigma_C}{\partial\Omega} (\epsilon_A I^A + \epsilon_B I^B), \tag{2}$$

where

$$I^A = e^{-(\int_A^S \mu dl + \int_S^B \mu' dl)} \int_A^S f dl,\ I^B = e^{-(\int_A^S \mu' dl + \int_S^B \mu dl)} \int_S^B f dl. \tag{3}$$

Here, $\sigma_{AS}$ and $\sigma_{BS}$ are geometrical cross-sections of the detectors $A$ and $B$, $f$ is the emitter activity, $\mu = \mu(E, S)$ is the linear attenuation coefficient depending on the photon energy $E$ and the scatter point $S$, $\epsilon_A = \epsilon_{AS}\epsilon'_{BS}$ and $\epsilon_B = \epsilon'_{AS}\epsilon_{BS}$ are related to the detection efficiency for the detectors $A$ and $B$, $\frac{\partial\sigma_C}{\partial\Omega}$ is the differential cross-section. Primed and unprimed quantities are evaluated at the scattered and unscattered photon's energy, respectively.

Equation (2) is symmetric in terms of $A$ and $B$ so that primary photons are recorded both at $A$ and $B$. We try to modify formula (2) within idealized assumptions on excellent energy resolution of pointwise detectors. Therefore a one-sided version of (2) is investigated, where only one detector $A$ is tuned to counting the primary photons. In this case, we can set $I^B = 0$ in (3). Let us denote, omitting other dependencies,

$$Q_{f,\mu}(x, y, z) \equiv \frac{\mu}{\sigma_C} \frac{\partial\sigma_C}{\partial\Omega} \epsilon_A e^{-(\int_A^S \mu dl + \int_S^B \mu' dl)} \int_A^S f dl, \tag{4}$$

where $(x, y, z)$ are Cartesian coordinates of the scatter point $S$. Thus, we transform equation (2) to the more compact form

$$S_V^{AB} = \iiint_V dV \left(\frac{\sigma_{AS}\sigma_{BS}}{4\pi|AS|^2|BS|^2}\right) Q_{f,\mu}(x, y, z). \tag{5}$$

This equation is a starting point for derivation both of total and sample Compton scatters at a certain angle.

### B. Geometrical Model of the Compton Single Scatter

The SSS approximation is sufficiently generic to deal with the scatter volume $V$ (or, equivalently, an integration domain, or a support of the attenuation map $\mu$) of an arbitrary shape. However, for the purposes of this research, a precise boundary of the $V$ (and the limits in volume integral (5)) should be explicitly specified as well as a system of coordinates needs to be chosen. The following basic geometrical observations are useful in analytical single scatter modeling.

Let us assume that the detectors $A$ and $B$ are small disks of radius $\delta \ll 1$. It is easily seen (Figure 2) that all the scatter points $S$ (with some scattering energy $E'$, or scattering angle $\theta$) are located on an equi-scatter surface (denoted as $\Sigma_\theta$) of the football-shape rotation body (denoted as $V_\theta$) generated by the arcs $\widehat{ASB}$ with the detectors $A$ and $B$ fixed. The arcs are parts of the circles with diameter $d = |AB|/\sin\theta$.

Let us assume that the detector $B$ records the photons scattered under the scattering angles $\theta$ such that $\theta \le T$, for some thresholding angle $T \le \pi/2$. We find it useful to exploit the spherical coordinates $(\psi, \varphi, r)$ with the origin at the point $A$ for describing the total scatter volume $V_T$ and the equiscatter surface $\Sigma_\theta$:

$$\begin{aligned} V_T &= \{(\psi, \varphi, r) |\, \psi \in [0, 2\pi), \phi \in [0, T], r \in [0, |AS|], \} \\ \Sigma_\theta &= \{(\psi, \varphi, r) |\, \psi \in [0, 2\pi), \phi \in [0, \theta], r = |AS|\}. \end{aligned} \tag{6}$$

Let us recall the Law of Sines for $\triangle ABS$

$$|AS|/\sin(\theta - \varphi) = |BS|/\sin(\varphi) = d. \tag{7}$$

It can be shown that

$$|AS| = |AB|\frac{\sin(\theta - \varphi)}{\sin\theta},\ |BS| = |AB|\frac{\sin\varphi}{\sin\theta}. \tag{8}$$

The term $\int_A^S f dl$ is of multiple use in the scatter calculations. For any scatter point $S$, it is expressed as follows

$$\int_A^S f dl = \int_0^{|AS|} f(\psi,\varphi,r)dr = \int_0^{|AB|\frac{\sin(\theta-\varphi)}{\sin\theta}} f(\psi,\varphi,r)dr. \quad (9)$$

The idealized model for the total scatter (parameterized by the threshold $T$ and denoted as $S_T^{AB}$) will be developed using the SSS integral (5) calculated at points within the small detectors $A$ and $B$, and then averaged over $(A,B)$ disks area as follows

$$S_T^{AB} = \lim_{\delta\to 0} \frac{1}{(\pi\frac{\delta^2}{4})^2} \int_A dA \int_B dB \iiint_{V_T} dV_T \times \left(\frac{\sigma_{AS}\sigma_{BS}}{4\pi|AS|^2|BS|^2}\right) Q_{f,\mu}(x,y,z). \quad (10)$$

The geometrical cross-sections of $A$ and $B$ incident to the rays $AS$ and $SB$ are respectively

$$\sigma_{AS} \approx (\pi\delta^2/4)\cos\varphi,\ \sigma_{BS} \approx (\pi\delta^2/4)\cos(\theta-\varphi). \quad (11)$$

Substituting (11) into (10), we estimate the total single scatter in the following form

$$S_T^{AB} = \iiint_{V_T} dV_T \left(\frac{\cos\varphi\cos(\theta-\varphi)}{4\pi|AS|^2|BS|^2}\right) Q_{f,\mu}(x,y,z). \quad (12)$$

We change the rectangular variables $(x,y,z)$ in (12) for other (spherical-like) curvilinear coordinates $(\psi,\varphi,\theta)$, where $\psi,\varphi$ are the spherical coordinates and $\theta\in[0,T]$ is the scattering angle (while the distance $|AB|$ is fixed), as follows

$$\begin{aligned} x &= X(\psi,\varphi,\theta) = |AS|\sin\varphi\cos\psi,\\ y &= Y(\psi,\varphi,\theta) = |AS|\sin\varphi\sin\psi,\\ z &= Z(\psi,\varphi,\theta) = |AS|\cos\varphi. \end{aligned} \quad (13)$$

For changing variables in (12), we calculate the elementary volume

$$dV_T = dxdydz = |J|d\psi d\varphi d\theta, \quad (14)$$

where $J$ is the Jacobian matrix

$$J = \begin{bmatrix} \partial X/\partial\psi & \partial X/\partial\varphi & \partial X/\partial\theta \\ \partial Y/\partial\psi & \partial Y/\partial\varphi & \partial Y/\partial\theta \\ \partial Z/\partial\psi & \partial Z/\partial\varphi & \partial Z/\partial\theta \end{bmatrix} \quad (15)$$

and $|J|$ is its determinant. Due to (8), we have

$$|J| = \frac{|AB|^3\sin^2(\varphi)\sin^2(\theta-\varphi)}{\sin^4(\theta)} = \frac{|AS|^2|SB|^2}{|AB|}, \quad (16)$$

and (12) becomes

$$\begin{aligned} S_T^{AB} &= \iiint_{V_T} d\psi d\varphi d\theta\,|J|\,\frac{\cos\varphi\cos(\theta-\varphi)}{4\pi|AS|^2|BS|^2} Q_{f,\mu}(\psi,\varphi,\theta)\\ &= \int_0^{2\pi} d\psi \int_0^T d\theta \int_0^\theta d\varphi\,\frac{\cos\varphi\cos(\theta-\varphi)}{4\pi|AB|} Q_{f,\mu}(\psi,\varphi,\theta). \end{aligned} \quad (17)$$

Finally, we derive the total scatter equation under further idealized assumptions $\epsilon_A \equiv 1$ in the following integral form:

$$S_T^{AB} = \int_0^T d\theta \int_0^\theta d\varphi \frac{\cos\varphi\cos(\varphi-\theta)}{4\pi|AB|} \int_0^{2\pi} d\psi\,\frac{\mu(\psi,\varphi,|AS|)}{\sigma_C} \times \frac{\partial\sigma_C}{\partial\Omega}\, e^{-\left(\int_A^S \mu dl + \int_S^B \mu' dl\right)} \int_0^{|AS|} f(\psi,\varphi,r)dr. \quad (18)$$

Let us represent equation (18) in the form

$$S_T^{AB} = \int_0^T \xi_\theta^{AB} d\theta, \quad (19)$$

where the integrand

$$\xi_\theta^{AB} = \int_0^\theta d\varphi \frac{\cos\varphi\cos(\varphi-\theta)}{4\pi|AB|} \int_0^{2\pi} d\psi \frac{\mu(\psi,\varphi,|AS|)}{\sigma_C} \times \frac{\partial\sigma_C}{\partial\Omega}\, e^{-\left(\int_A^S \mu dl + \int_S^B \mu' dl\right)} \int_0^{|AS|} f(\psi,\varphi,r)dr \quad (20)$$

is a sample value of the scatter. Here $\theta$ and $E'$ are fixed, therefore the factor $\frac{1}{\sigma_C}\frac{d\sigma_C}{d\Omega}$ in (20) is a scalar and for brevity can be omitted without loss of generality .

### C. Slice-by-slice Convolution Blurring Model

An essential simplification can be achieved assuming $\mu = const$. Then equation (20) can be written down in the cylindrical coordinates $(\psi,\rho,z)$ after some algebra as follows

$$\xi_\theta^{AB} = \frac{\mu}{4\pi|AB|} \int_0^{|AB|} dz \int_0^{R_\theta(z)} d\rho \frac{z(z\cos\theta+\rho\sin\theta)}{\rho(z^2+\rho^2)^{3/2}} \times e^{-\frac{|AB|\mu}{\sqrt{z^2+\rho^2}}(z+\rho\tan(\theta/2))} \int_0^{2\pi} d\psi f(\psi,\rho,z), \quad (21)$$

where radius of the circular section of $V_\theta$ with the coordinate $z$ is

$$R_\theta(z) = \frac{\sqrt{a^2-(z-a)^2\sin^2\theta} - a\cos\theta}{\sin\theta},\ a \equiv \frac{|AB|}{2}. \quad (22)$$

Multiplying equation (21) by $1 \equiv \rho/\rho$ and denoting the kernel

$$h_\theta(\rho,z) \equiv \frac{\mu}{4\pi|AB|} \frac{z(z\cos\theta+\rho\sin\theta)}{\rho^2(z^2+\rho^2)^{3/2}} e^{-\frac{|AB|\mu(z+\rho\tan(\theta/2))}{\sqrt{z^2+\rho^2}}}, \quad (23)$$

we can reduce (21) to

$$\xi_\theta^{AB} = \int_0^{|AB|} dz \int_0^{2\pi} d\psi \int_0^{R_\theta(z)} h_\theta(\rho,z) f(\psi,\rho,z)\rho d\rho. \quad (24)$$

It follows from this representation that the inner double integral $\int_0^{2\pi} d\psi \int_0^{R_\theta(z)} h_\theta(\rho,z) f(\psi,\rho,z)\rho d\rho$ in (24) is a value of the convolution of the function $f$ section by the plane parallel

to $xOy$ with the coordinate $z$, and the radially symmetric kernel $h_\theta(\rho, z)$ with a circular support of radius $R_\theta(z)$. The outer integral $\int_0^{|AB|} dz$ represents the X-ray transform of the slice-by-slice blurred version of the activity function $f$ along the lines parallel to the direction $z$. This slice-by-slice distance-dependent blurring model of the projection formation is known in Transmission Electron Microscopy and it is proven to be invertible [7] provided full data are available. The reconstruction technique derived was named as the Defocus-gradient Corrected Backprojection (DGCBP) algorithm. Thus, we have reduced the simplified Compton scatter model to the already developed reconstruction algorithm. This algorithm was numerically tested [7] by simulating different types of noise based on the principles proposed by Baxter et al. [8]. Theoretical study of the noise propagation properties of the scatter forward transform (20) is a subject of the future research.

Let us introduce the Fourier transform pairs: $F(k_1, k_2, k_3) = \mathcal{F}_3\{f(x, y, z)\}$, $H_\theta(k_1, k_2, z) = \mathcal{F}_2\{h_\theta(\rho, z)\}$, and $P_\theta^{\alpha,\beta} = \mathcal{F}_2\{\xi_\theta^{\alpha,\beta}\}$. Here $\xi_\theta^{\alpha,\beta}$ is a scatter projection in the direction specified by the unit vector parameterized by the spherical angles $(\alpha, \beta) \in \mathbb{S}^2$. The scatter projection $\xi_\theta^{\alpha,\beta}$ is a collection of the scatter forward transform (20) samples $\xi_\theta^{AB}$, where the points $A$ and $B$ belong to the lines that constitute a bundle of parallell lines in the direction $(\alpha, \beta)$. The DGCBP algorithm consists of the following steps.

Step 1. Deconvolution of the projection $P_\theta^{\alpha,\beta}$ with the Tikhonov regularized inverse filter and stacking the results along $z$ for all directions $(\alpha, \beta) \in \mathbb{S}^2$:

$$b_\theta^{\alpha,\beta}(x, y, z) = \mathcal{F}_2^{-1}\Big\{\frac{P_\theta^{\alpha,\beta}(k_1, k_2)\, H_\theta(k_1, k_2, z)}{H_\theta(k_1, k_2, z)^2 + \lambda(k_1^2 + k_2^2)}\Big\}. \quad (25)$$

Step 2. Generation of the integral image $c_\theta(x, y, z)$ as summation of the backprojections $b_\theta^{\alpha,\beta}$ over all the projection directions $(\alpha, \beta) \in \mathbb{S}^2$:

$$c_\theta(x, y, z) = \iint_{\mathbb{S}^2} b_\theta^{\alpha,\beta}(x, y, z) \partial\alpha\partial\beta. \quad (26)$$

Step 3. Ramp-filtering in the Fourier domain of the integral image $C_\theta(k_1, k_2, k_3) = \mathcal{F}_3\{c_\theta(x, y, z)\}$:

$$F(k_1, k_2, k_3) \approx C_\theta(k_1, k_2, k_3) \times \sqrt{k_1^2 + k_2^2 + k_3^2}. \quad (27)$$

## III. Simulation study

The numerical experiments were performed using a numerical test phantom of $256^3$ size. It consists of 7 and 11 spheres serving as a support of the activity function $f \equiv 1$ immersed into a larger sphere filled with water with the linear attenuation coefficient $\mu = 0.096 cm^{-1}$ (Figure 3 (a)). Images of three central sections are shown in Figure 3 (b) of the test object (the upper row), and of the reconstruction (the bottom row) from $1,000$ scatter projections randomly oriented over $\mathbb{S}^2$. Projections of $256 \times 256$ size each beeing numerically generated with a scattering angle $\theta = 30^\circ$ using formula (20). The regularization parameter $\lambda = 0.01$ of the Tikhonov filter is used in the DGCBP algorithm, Step 1, equation (25).

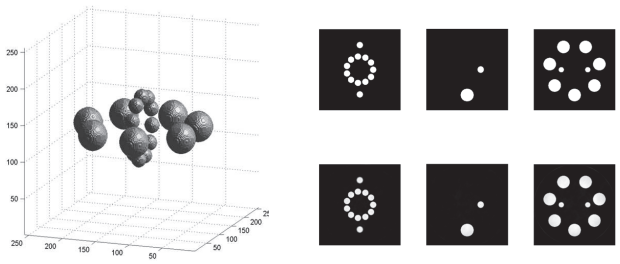

(a) (b)

Fig. 3. (a) The 3D view of a test object with 7 and 11 spheres of the unit activity immersed into the imaginable sphere filled with water and digitized into an image of $256^3$ size. (b) Images of three central sections of the test object (the upper row), and the DGCBP reconstruction (the bottom row) from $1,000$ randomly chosen scatter projections.

## IV. Conclusion

The closely related integral transforms (18) and (20) describing the total and sample single scatter projection formation have been derived from the classical SSS approximation (2). The single scatter image formation includes integration of the emitter activity $f$ over a bundle of compound cones with a common vertex at the point $A$. Those cone integrals are weighted by the linear attenuation $\mu$ and some geometrical factors. We can conclude therefore that the integral transforms obtained belong to the family of the Compounded Conical Radon Transforms [4]. With some improvements in the detector energy resolution, the energy-selected PET could be a source of the new opportunities.

## Acknowledgments

We thank Drs. Robert Lewitt and Samuel Matej for fruitful discussions. This work was partially supported during the stay of the first author with the Department of Physics of the Technical University of Denmark.

## References

[1] S. Norton, "Compton scattering tomography", *Journal of Applied Physics*, vol. 76, no. 4, pp. 2007–2015, 15 August 1994.
[2] G. Rigaud, M. K. Nguyen and A. K. Louis, "Modeling and simulation results on a new Compton scattering tomography modality," *Simulation Modeling: Practice and Theory*, vol.33, pp. 28–44, April 2013.
[3] H. Zaidi, "Scatter modelling and correction strategies in fully 3-D PET," *Nuclear Medicine Communications*, vol. 22, pp. 1181–1184, 2001.
[4] M. K. Nguyen, T. T. Truong, C. Driol and H. Zaidi, "On a Novel Approach to Compton Scattered Emission Imaging," *IEEE Trans. Nucl. Sci.*, vol. 56, no. 3, pp. 1430–1437, June 2009,
[5] Th. Koesters, "Derivation and Analysis of Scatter Correction Algorithms for Quantitative Positron Emission Tomography", Disseration Thesis, Muenster University, 2010.
[6] C. C. Watson, "New, faster, image-based scatter correction for 3D PET," *IEEE Trans. Nucl. Sci.*, vol. 47, pp. 1587–1594, 2000.
[7] I. G. Kazantsev, J. Klukowska, G. T. Herman, and L. Cernetic, "Fully three-dimensional defocus-gradient corrected backprojection in cryo-electron microscopy", *Ultramicroscopy*, vol. 110, pp. 1128–1142, 2010.
[8] W. T. Baxter, R. A. Grassucci, H. Gao, and J. Frank, "Determination of signal–to–noise ratios and spectral SNRs in cryo–EM low–dose imaging of molecules", *Journal of Structural Biology*, vol. 166, pp. 126–132, 2009.